INTERNATIONAL JOURNAL OF AUTOMOTIVE AND MECHANICAL ENGINEERING
ISSN: 2229-8649 e-ISSN: 2180-1606
VOLUME 22, ISSUE 3, 2025, 12586 - 12602
DOI: https://doi.org/10.15282/ijame.22.3.2025.4.0961

RESEARCH ARTICLE

Longitudinal Dynamics Modeling of an Electric Go-Kart and Analysis of Regenerative Braking under Various Braking Profiles using MATLAB Simulink

K. A. Tofrowaih[1,2], M. Abdullah[1]*, S. F. Toha[3], A. Rahman[4]

[1]Department of Mechanical and Aerospace, Faculty of Engineering, International Islamic University Malaysia, Jalan Gombak, 53100, Kuala Lumpur, Malaysia

[2]Faculty of Mechanical Technology and Engineering, Universiti Teknikal Malaysia Melaka, Hang Tuah Jaya, 76100 Durian Tunggal, Melaka, Malaysia

[3]Department of Mechatronics, Faculty of Engineering, International Islamic University Malaysia, Jalan Gombak, 53100, Kuala Lumpur, Malaysia

[4]12GameAbove Engineering and Technology, Eastern Michigan University, Ypsilanti, MI, USA 48197

ABSTRACT – Regenerative braking plays a crucial role in optimizing energy efficiency in electric vehicles (EVs), yet its performance is significantly influenced by driving behavior. This study investigates the impact of various braking profiles on regenerative braking effectiveness, with a focus on battery State of Charge (SOC) recovery. As a proof of concept, a control-oriented, first-principles mathematical model of an electric go-kart was developed in MATLAB Simulink using real prototype parameters to simulate longitudinal vehicle dynamics under different throttle, coasting, and braking conditions. In this setup, the vehicle employs a simple Regenerative Braking System using a direct current motor, which is activated when the throttle pedal is released and operates with a constant Back Electromotive Force (EMF) resistance. This mechanism can slow down the vehicle, but a friction brake is still required for a complete stop. Open-loop simulation results show that full-throttle driving achieves a maximum speed of 13.7 m/s, resulting in a 1.16% SOC depletion. During coasting, when regenerative braking is active, a 0.05% SOC gain was recorded over 100 seconds. For braking applications, the highest energy recovery (+0.030% SOC) occurred with a strategy involving 4 seconds of coasting followed by strong braking; however, this induced a high deceleration of -11.7 m/s², potentially affecting ride comfort. In contrast, immediate light braking without coasting resulted in a lower deceleration of -3.4 m/s² but reduced SOC recovery to 0.023%. These results emphasize the trade-off between energy recovery and ride comfort, underscoring the need for intelligent, adaptive braking strategies in future compact EV designs, particularly where integration with autonomous braking systems is anticipated.

ARTICLE HISTORY

Received	:	24th Sept. 2024
Revised	:	04th June 2025
Accepted	:	30th June 2025
Published	:	01st Sept. 2025

KEYWORDS
Electric Go-Kart
Longitudinal dynamics
Mathematical modelling
Regenerative braking

1. INTRODUCTION

As environmental concerns continue to intensify, there is a huge interest in the automotive sector toward Electric Vehicles (EVs) for more sustainable and efficient transportation. However, one of the persistent challenges faced by battery-based EVs is their limited range. To address this issue, various strategies have been developed to optimise energy usage, such as improving the Battery Management System (BMS) [1], [2], Thermal Management System [3–6], and power electronics system [7–9]. Nevertheless, one of the simplest methods is the Regenerative Braking System (RBS) [10–18], which transforms the kinetic energy during coasting into electrical energy and stores it in the vehicle's battery. This extends the driving range and improves overall vehicle efficiency while reducing the wear on the brake pads.

Mamgai [19] provided a comprehensive overview of the RBS mechanism, including those utilising electric motors, flywheel-based systems (f-RBS), and hydraulic RBS. Ji et al. [10] further identified that kinetic energy recuperation in EVs can occur under three distinct conditions: during deceleration when the Accelerator Pedal (AP) is released, during braking when the Brake Pedal (BP) is applied, and during free rolling when both AP and BP are fully disengaged. Common RBS control strategies include the Combined Serial RBS (SRBS) and the Combined Cooperative RBS (CRBS). SRBS is characterised by its simplicity and lower cost, making it suitable for low-deceleration applications. In SRBS, braking initially relies solely on regenerative braking, transitioning to friction braking once a predefined threshold is exceeded. However, its braking torque is inherently speed-dependent, which may limit its effectiveness at lower speeds. In contrast, CRBS requires coordinated control of both friction and regenerative braking systems, increasing system complexity. Nevertheless, it offers speed-independent braking and enables greater energy recuperation by fully leveraging the electric braking potential [20]. For simplicity, this work adopts simple RBS using a direct current (DC) motor, which is activated when the throttle pedal is released and operates with a constant Back Electromotive Force (EMF) resistance. This mechanism can slow down the vehicle, but a manual friction brake is still required for a complete stop.

Despite the energy-saving benefits of RBS, their effectiveness is highly dependent on how friction braking is applied. Braking too late can cause passenger discomfort due to abrupt deceleration [21], while braking too early limits energy recovery by dissipating kinetic energy through friction brakes [22]. However, there is a lack of quantitative analysis on

*CORRESPONDING AUTHOR | M. Abdullah | ✉ mohd_abdl@iium.edu.my

how specific braking profiles, such as combinations of coasting and friction braking, affect both energy recovery and ride comfort for small-scale EVs. This study addresses this problem statement by modelling and analysing different braking strategies to analyse the effect of maximising energy recovery on passenger comfort. This analysis provides valuable insights and can serve as a reference for designing autonomous braking systems in future applications to further optimise the system's performance. To investigate this matter economically, a small-scale EV plant is desired for proof of concept. Thus, an electric go-kart is considered in this work as it has a straightforward powertrain system and can closely replicate the actual vehicle. This go-kart system has relatively modest performance capabilities, propelled by an electric motor and powered by a Lithium-ion battery. In addition, an RBS can be embedded to charge the battery with a suitable motor driver. Nevertheless, before running any actual hardware test, it is advisable to simulate the response in a virtual environment by developing a simple yet reliable mathematical model representing the real system [23], [24]. There are several uses of mathematical models, such as design optimisation [25], controller development [26], dynamic prediction, and performance analysis [27], [28], where the complexity of the model depends on the type of application. However, for control purposes, a simple yet reliable model is adequate for capturing only the essential dynamics of the real hardware.

In general, there are two modelling approaches, namely first principle (white box) and system identification (black box). A system identification model uses measured input-output data to identify the system dynamics without knowing the underlying relationship. For example, in the work of Wahid et al. [29], a system identification model is developed for Switch Reluctance Motor (SRM). Similarly, Hikono et al. [25] also use system identification to represent rechargeable battery performance in EVs. Besides, Sunori et al. [30] also developed a mathematical model for the overall electric vehicle dynamics using system identification. In the study by Buggaveeti et al. [31], system identification was applied to a Toyota Prius Plug-in Hybrid Electric Vehicle (PHEV) to estimate key vehicle parameters. The results demonstrated that the proposed estimation methods were capable of accurately identifying parameters such as frontal area, rolling resistance coefficient, center of gravity location, suspension stiffness and damping, wheel inertia, tire model coefficients, and half-shaft stiffness, with sufficient precision for modeling and simulation purposes. Although the method seems easy, the implementation is not that straightforward. First, a detailed experimentation setup is needed to obtain suitable training and validation data. Second, there is no standardised method for the training process where a user needs to select from a vast number of choices, such as the order of the model and types of models. The model is also not generalised since it is system dependent. Besides, it requires many trial and error processes to avoid model overfitting or underfitting.

On the other hand, the first principal model assumes that the internal system dynamics are recognisable and derivable. For example, in the work of Gulzar et al. [26], the first principal technique is used to construct a complete vehicle dynamics model of an EV, which consists of the equations for vehicle dynamics, motor, battery, braking, transmission, and others. Mohd et al. [32] also employed a first-principles approach, developing a fundamental mathematical model and simulation of a full-scale battery electric vehicle using the MATLAB-Simulink platform to analyze power flow during both motoring and regenerative modes. The model primarily consisted of the electric motor, controller, battery, and a proportional-integral (PI) controller to compensate for battery voltage error. The main challenge in constructing this model is to obtain its parameters and coefficients, where manual measurement and experimental work are needed. However, a user can have a deep understanding of the impact of each parameter on the vehicle's performance. Hence, it is quite suitable for design and optimisation work. Besides, it is easy to generalise for other types of vehicles just by changing the parameters and coefficients. While prior studies have extensively explored EV dynamics modelling through both system identification and first-principles approaches, ranging from component-level estimation in full-scale plug-in hybrid vehicles to comprehensive vehicle simulations, limited attention has been directed towards compact, low-inertia EV platforms such as electric go-karts, which can be used as a simple proof of concept plant. Additionally, current regenerative braking research often emphasizes full-scale or high-performance vehicles, with insufficient consideration of braking dynamics, energy recovery potential, and strategy suitability in smaller, lightweight EVs. Thus, a clear gap exists in developing simplified, yet precise first-principles models tailored specifically to small-scale EVs and systematically assessing regenerative braking strategies appropriate for these low-speed, low-inertia systems.

This work aims to address the identified gap by developing a control-oriented, first-principles model specifically designed for a small-scale electric go-kart platform. The objective is to analyse how different braking profiles affect RBS performance, specifically by evaluating their impact on the battery's State of Charge (SOC). The insights gained from this analysis aim to support the design of intelligent braking controllers for future work that maximise energy recovery while preserving ride comfort. The compact scale vehicle facilitates a detailed investigation of braking profile effects without the complexities inherent to larger vehicle systems. Furthermore, unlike existing literature, this work explicitly evaluates real-prototype parameters within a control-oriented model built in MATLAB Simulink.

2. METHODOLOGY

This section provides the methodology for this work, which starts with explaining a simple mathematical model to represent specific go-kart longitudinal dynamics that include the equations of the electric motor, brake, drivetrain, and vehicle body. Then, it continues with the explanation of electric equations to calculate the SOC of a battery. Most model parameters are measured or calculated based on the real prototype. However, certain parameters, which are difficult to measure, such as the coefficients, are taken from reputable references. The overall simulation architecture is shown in Figure 1. This model is developed based on the basic EV Simulink model setup from MATLAB reference [33] with several modifications. It is important to note that this study is purely theoretical, and no experimental validation was conducted at this stage; model validation is planned as part of future research.

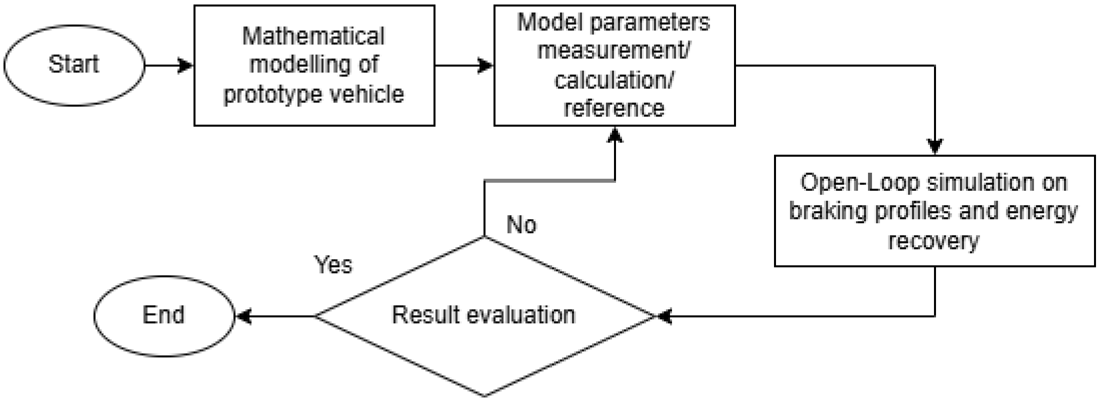

Figure 1. Overall simulation architecture

2.1 Direct Current Motor Equation

In this work, a 48 V Brushless Direct Current (BLDC) motor with 1,800 W is considered as the main power source to propel the go-kart, as shown in Figure 2. Although there are many ways to model this motor, the simplest one is to utilise the motor's measured maximum power and torque to establish the relationship between pedal pressing and motor torque. Figure 3 shows the dyno test setup on the motor that was used to plot the torque vs angular speed graph, as shown in Figure 4. Based on the graph, it is estimated that the maximum torque T_{max} that can be generated by this motor is around 9.971 Nm by using the polynomial approximation. As for the maximum power P_{max}, the specification given by the factory is 1,800 W. Figure 5 shows the Simulink block diagram for the motor that was developed in this work. The inputs to the block are the percentage of accelerator pedal pressing (APP), motor speed, and vehicle velocity, while the output is the motor net torque.

Figure 2. 1,800W DC motor for the go-kart

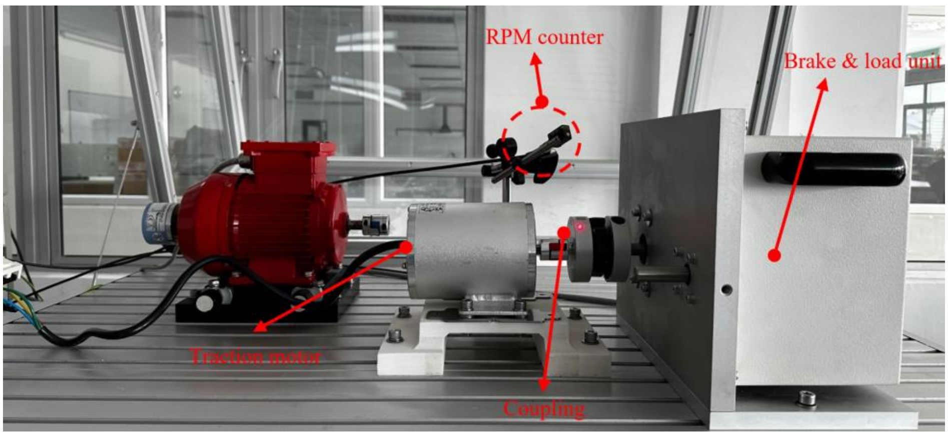

Figure 3. Experiment setup for traction motor torque-speed

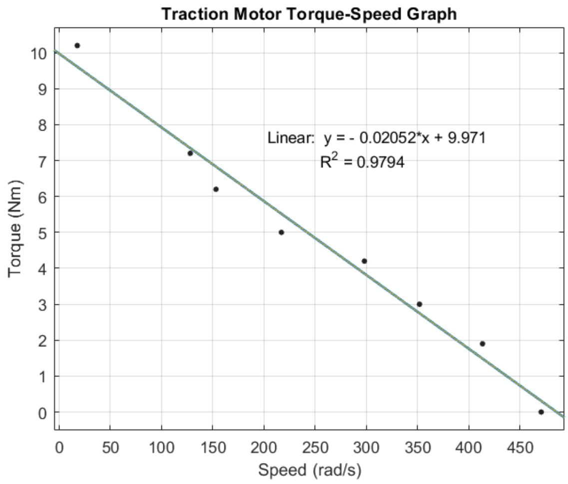

Figure 4. Traction motor torque-speed graph

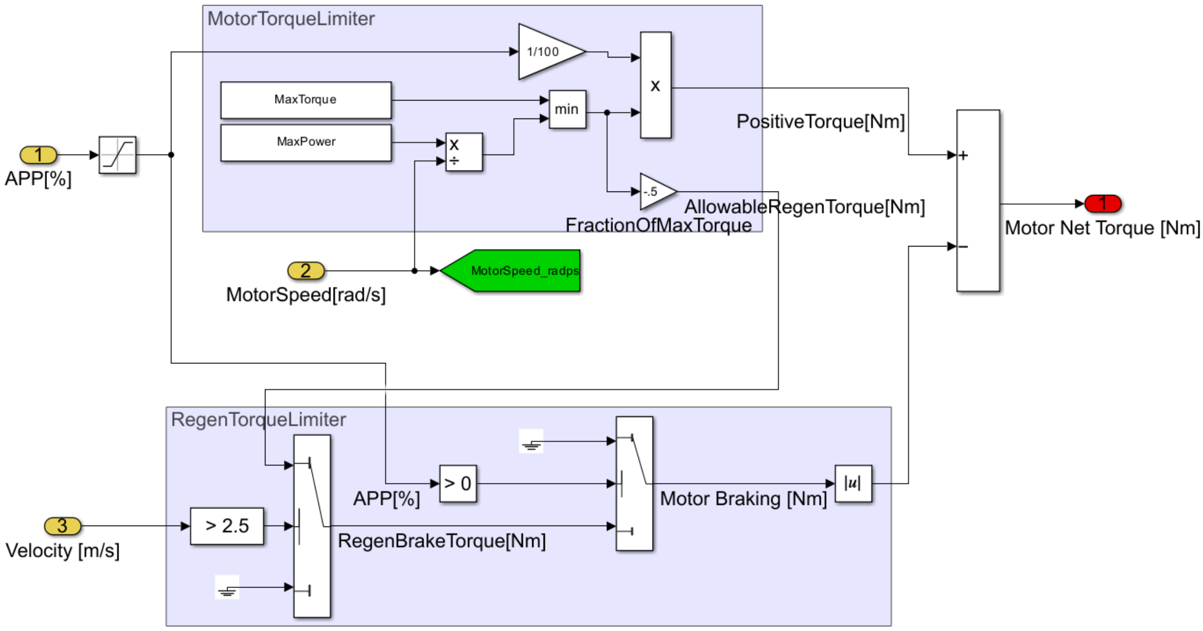

Figure 5. Motor subsystem

To estimate the instantaneous maximum torque produced by the motor at the current angular speed $T_{max@\omega}$, the lowest torque between the two previous estimated values, namely the maximum torque T_{max} and the maximum power P_{max} is taken, which can be described by this equation:

$$T_{max@\omega} = \min\left(T_{max}, \frac{P_{max}}{\omega}\right) \tag{1}$$

where ω is the instantaneous angular speed of the motor. Thus, the positive torque generated by the motor T_m can be mapped with the percentage of throttle-pressing x_t via this equation:

$$T_m = 0.1 x_t T_{max@\omega} \tag{2}$$

Since the DC motor can also act as a generator via the vehicle momentum when there is no voltage supplied to the motor, a negative torque, known as regenerative braking, T_{rbs}, can be calculated as:

$$T_{rbs} = -0.5 T_{max@\omega} \tag{3}$$

In this case, it is assumed that only 50% of the current torque can be used for RBS based on the maximum vehicle kinetic energy that could be converted into regenerative energy [34]. Nevertheless, this negative torque should only be considered when the velocity is more than 2.5 m/s and when the percentage of throttle pressing, x_t is zero. Equation 4 provides the conditions and Figure 5 shows its implementation in Simulink.

$$if\ v < 2.5\ and\ x_b = 0\%\ ;\ T_{rbs} = 0 \tag{4}$$

Finally, the net torque produced by the motor will be calculated as:

$$T_{m,net} = T_m + T_{rbs} \tag{5}$$

This net torque will be sent to the drive train block to calculate the traction force generated by the go-kart.

2.2 Drivetrain Equation

In general, the drivetrain is responsible for transferring the net torque, $T_{m,net}$ that is generated by the motor and sent to the wheel. The tractive force generated by the drivetrain can be calculated as:

$$F_t = \frac{G_r}{r_w}(T_{m,net} - T_{loss}) \tag{6}$$

where G_r is the gear ratio between the output gear and the input gear, r_w is the wheel radius and T_{loss} is the estimated mechanical torque loss encountered by the drive train that can be estimated by:

$$T_{loss} = \omega b \tag{7}$$

where b is the assumed damping coefficient of torque. The angular speed of the motor, ω can be estimated as:

$$\omega = v\frac{G_r}{r_w} \tag{8}$$

Given that v is the vehicle speed. In the simulation, the minimum value of motor speed ω, should be set to a small non-zero value to avoid numerical error, where, in this case, it is set to 0.00001 rad/s. Also, torque loss T_{loss}, should be constrained to zero when velocity is zero to avoid a negative value that can disturb the logical response of the model. Figure 6 shows the overall Simulink block for the drivetrain, where the inputs to the block are vehicle speed, net motor torque and brake force, while the tractive force is the output.

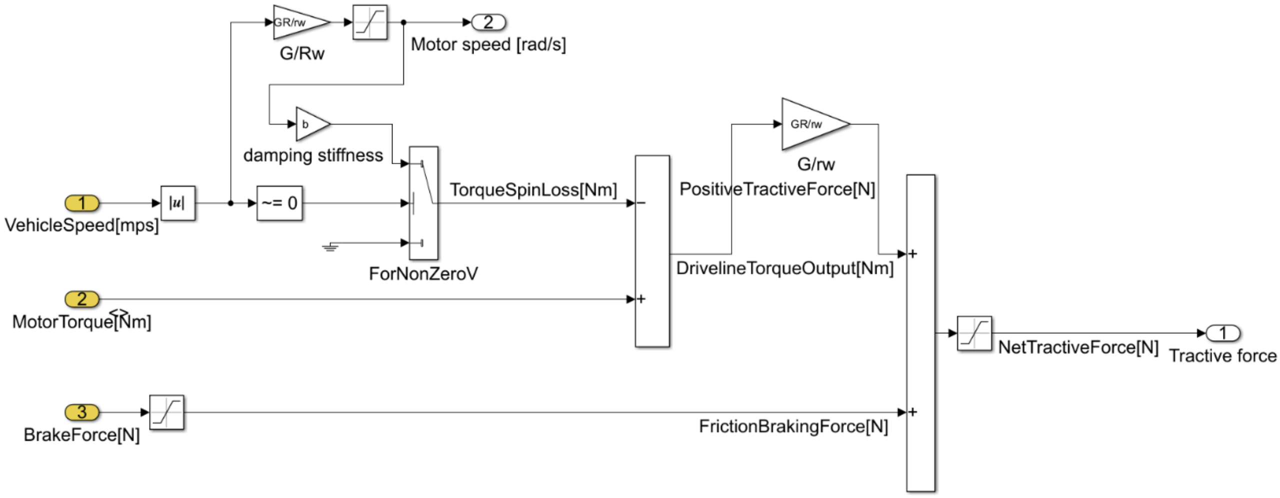

Figure 6. Drivetrain subsystem

Table 1 lists all the parameters used for the drivetrain equation, most of which are measured from the actual go-kart prototype. Figure 7 shows the sprocket configuration of the go-kart to measure the gear ratio between the drive and driven gears.

Table 1. Drivetrain model design parameter values

Parameter	Description (unit)	Values
b	Torque damping coefficient	0.004
G_r	Gear ratio	6.1935
r_w	Wheel radius (m)	0.15

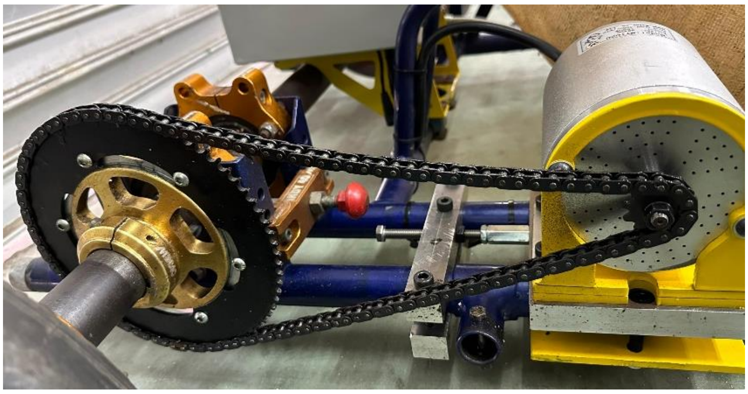

Figure 7. Sprocket configuration of the go-kart

2.3 Brake Equation

The input to the brake model is the percentage of brake pedal pressing (BPP), while the output is the brake torque. A full friction brake is used for the go-kart, as shown in Figure 8.

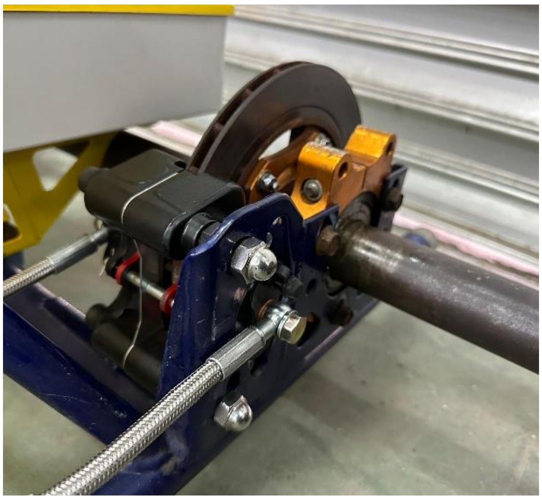

Figure 8. Go-kart friction brake system

According to Idros et al. [35], since the dynamic of the brake can be assumed linear, and most of the parameters in brake parts, such as brake actuator bore diameter, the outer and inner diameter of the brake pad, static and kinetic frictions, are all constants, the brake force F_b calculation can be simplified to:

$$F_b = k_b x_b \tag{9}$$

where k_b represents the assumed brake gain of 100, and x_b denotes the percentage of brake press. It is important to note that the brake input should be negative to yield a negative output since the brake always opposes the motion. Although most EVs integrate the motor braking and friction brake in their braking system, this work adopts a separate mechanism to match the prototype. Thus, the model does not include a proportional setting for friction braking and motor braking distribution. This work adopts an SRBS strategy, which is simpler in design to maximise SOC via coasting and only control friction braking. The regenerative braking torque is applied at a constant level during initial BP application, and only the friction braking torque is proportioned based on pedal input beyond a defined threshold. This approach was selected to reflect the actual implementation in the go-kart prototype, which lacks integrated motor-friction brake coordination hardware. While this simplification may reduce the model's resemblance to advanced EV systems with fully blended braking, it provides a more realistic representation of basic electric drive platforms and reflects the capabilities of our in-house prototype, for which this is the first custom-developed model. Moreover, it ensures consistent regenerative performance and isolates the influence of friction braking, enabling clearer analysis of braking profile effects on energy recovery and ride comfort. Figure 9 illustrates the Simulink block of the brake system.

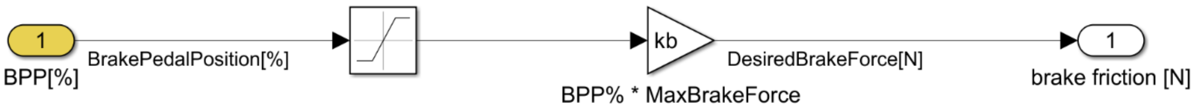

Figure 9. Brake subsystem

2.4 Vehicle Body Equation

Vehicle body dynamics consists of several important forces that can affect the movement of a vehicle. The input to this block is the tractive force F_t and brake force F_b, while the output is the vehicle's velocity, v. By referring to Figure 10, the motion of the vehicle is resisted by several forces, such as the aerodynamic force F_a, rolling resistance force F_r, and gradient force F_g.

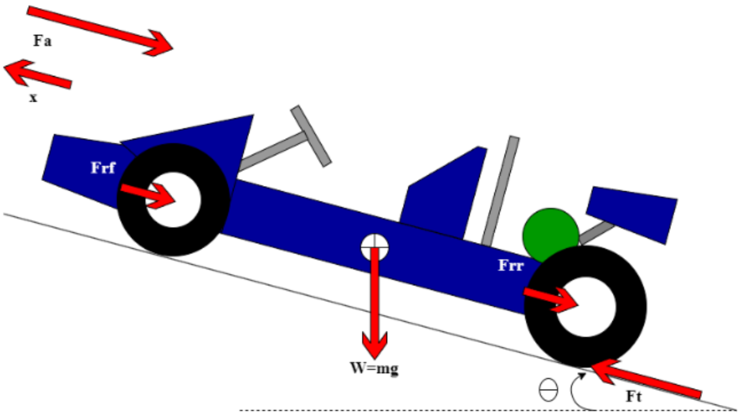

Figure 10. Simplified vehicle longitudinal model

The overall equation can be represented by utilising Newton's 2nd law by summing all the forces and equating it to the inertial force, such as:

$$F_t - F_b - F_a - F_r - F_g = m\ddot{x} \tag{10}$$

where m is the mass of the vehicle and $\ddot{x}$ is the acceleration. The vehicle velocity can be obtained by integrating the acceleration as shown in the Simulink block in Figure 11.

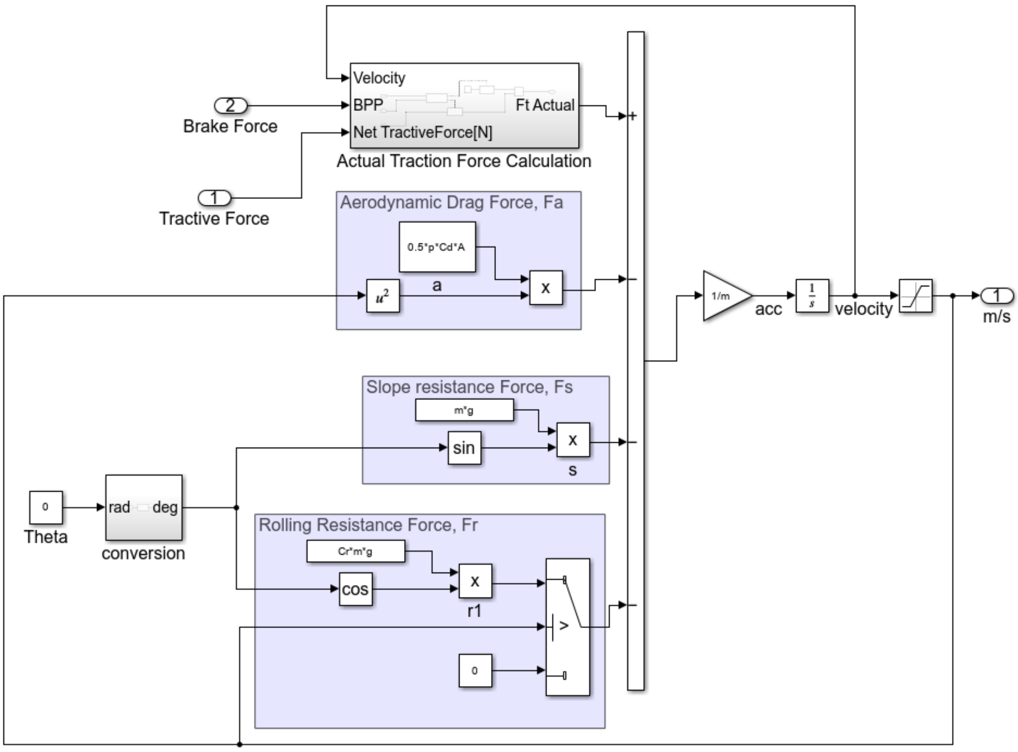

Figure 11. Vehicle dynamics subsystem

The equation for each force is derived based on the free body diagram given in Figure 10, and according to the standard references [36], [37], the equations are given below:

$$F_a = 0.5\rho C_d A_f v^2 \tag{11}$$

$$F_r = \mu_k mg\cos\theta \tag{12}$$

$$F_g = mg\sin(\theta) \tag{13}$$

Most of the parameters in Equations (11), (12), and (13) are measured from the go-kart, while some of them, such as the coefficient, are taken from the standard value based on standard vehicle dynamics literature [36]. Table 2 provides the values for the parameters used for the vehicle body equation. The vehicle load mass m, inclusive of the driver's mass, is considered alongside the go-kart's chassis, powertrain, and electrical system. For simplicity, the frontal area, A_f of the Go-Kart is approximated as a substantial rectangular shape. The area under scrutiny is estimated and graphically represented as a yellow rectangle and a hatched red polygon in Figure 12, which signifies the area that is not considered. This approximation allows for a more manageable analysis while maintaining a reasonable degree of accuracy.

Table 2. Model design parameter values

Parameter	Description (unit)	Values	Source
ρ	Air density (kg/m^3)	1.2250	Rajamani [36]
C_d	Drag coefficient	0.2	M. Abdullah et al. [38]
A_f	Vehicle frontal area (m^2)	0.66	Measured Estimation
μ_k	Rolling resistance coefficient	0.015	Rajamani [36]
m	Vehicle load mass (kg)	150	Measured
g	Gravity acceleration (m/s^2)	9.81	Standard

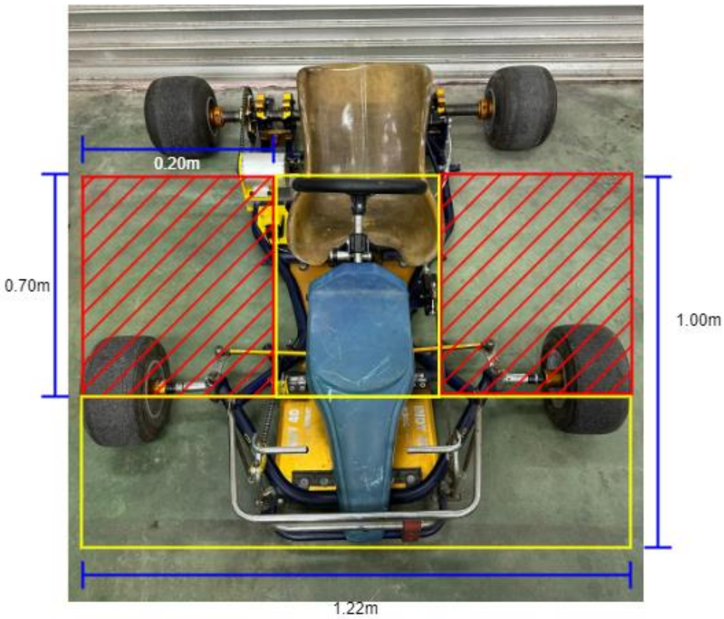

Figure 12. Estimation of the frontal area of the Go-Kart

It is also important to use a conditional limiter to avoid the negative velocity value. If the summation of force is negative (mostly due to the large value of braking force), the velocity will also become negative. By default, the negative velocity means the car is moving in the opposite direction, but the vehicle is stopped in real situations. To overcome this issue, a minor adjustment in the traction force is applied, as shown in Figure 13. If the velocity is zero or negative and the percentage of brake press is more than zero, then the total traction force should be equal to zero. Otherwise, the total traction force remains the same.

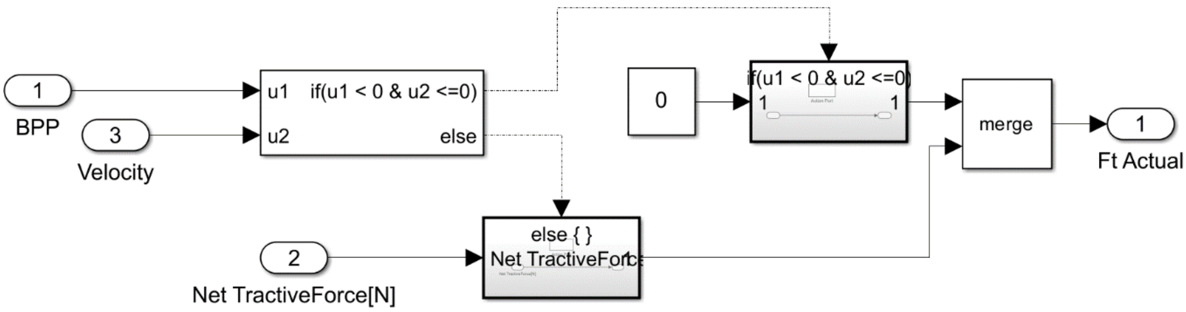

Figure 13. Actual traction force calculation

The same concept is applied to the rolling resistance because this parameter should only have a value when the vehicle is moving, as shown in the bottom part of Figure 11. Without the condition, the cosine function will provide a value (Note that $cos\ 0 = 1$) even if there is no input from the throttle. Thus, the condition is set such that if the velocity is more than zero, the switch is active, but when the velocity is equal to zero, the overall value for rolling resistance force should be equal to zero. These two sets of conditions are important to ensure that the traction force produced by the model is always positive.

2.5 State of Charge Equation

The previous equations are enough to simulate the overall vehicle motion. However, the equation that describes the State of Charge (SOC) needs to be analysed. The relationship can be obtained from the power input in Equation (5) of the motor, such that

$$P_{in} = T_{m,net}\omega + P_{loss} \tag{14}$$

where P_{in} is the supplied input power from the battery and P_{loss} is the estimated power loss that can be calculated from the motor efficiency given by the manufacturer, which is η = 0.8 as:

$$P_{loss} = (T_{m,net}\omega/\eta) - T_{m,net}\omega \tag{15}$$

Since power is supplied from a battery, by using the electrical equation, it is noted that $P_{in} = P_{actual} + P_{loss}$. This power loss is due to the internal resistance of the battery, and thus:

$$P_{in} = IV_{oc} - I^2R_{int} \tag{16}$$

where I is the supplied current, V_{oc} is the open circuit voltage, and R_{int} is the internal resistance of the battery. It is noted that Equation (16) is in the form of a quadratic function, and hence, the supplied current can be calculated as:

$$I = \frac{V_{oc} - \sqrt{V_{oc}^2 - 4R_{int}P_{in}}}{2R_{int}} \tag{17}$$

Once the supplied current value is calculated, the state of charge can be estimated via this equation:

$$SOC = -\left(\int IV_{oc}\right)\frac{1}{3600 * 1000C} \tag{18}$$

The integral represents the energy dissipated over a given time interval. Where C denotes the battery's energy capacity measured in watt-hours (W.h). SOC can be determined by dividing the energy dissipated by the energy capacity. Figure 14 shows the Simulink block and Table 3 provides all the parameters used in the simulation for the SOC equation. Finally, Figure 15 illustrates the overall schematic diagram of the electric go-karts that include all the subsystems.

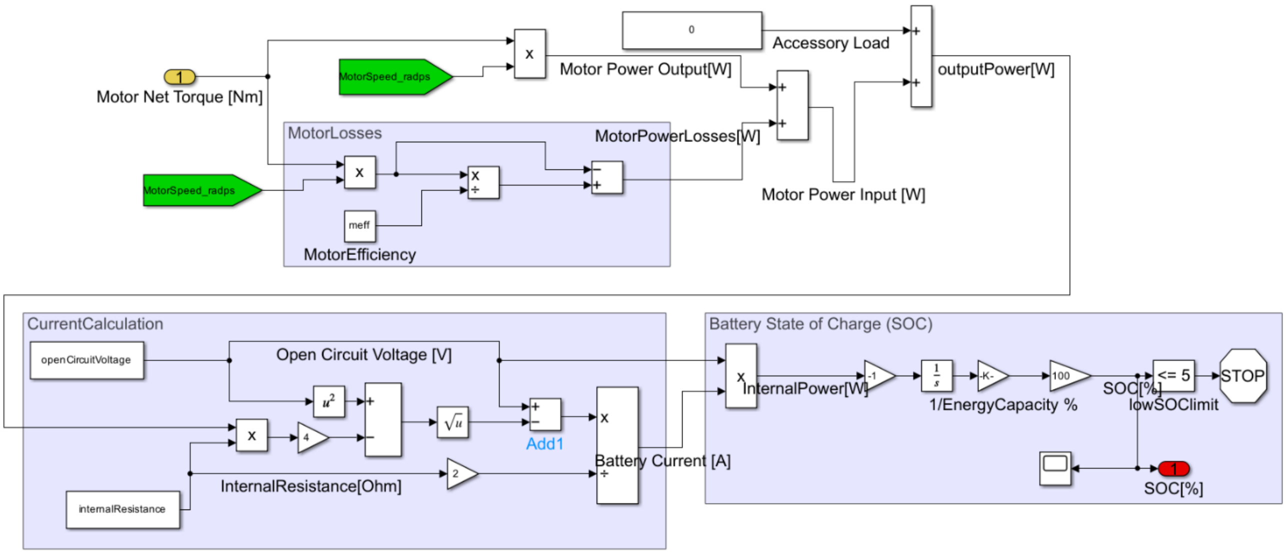

Figure 14. Battery subsystem

Table 3. Battery subsystem model design parameter values

Parameter	Description (unit)	Values
V_{oc}	Open Circuit Voltage (V)	48
R_{int}	Battery internal resistance (Ω)	0.1
C	Battery energy capacity (kWh)	5

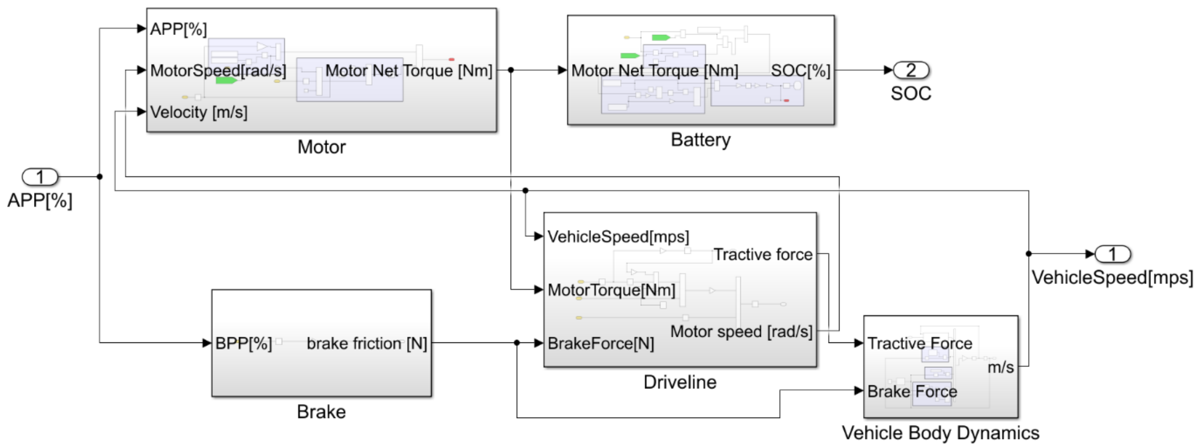

Figure 15. Electric Go-kart schematic diagram

3. RESULTS AND DISCUSSION

This section discusses the simulation results together with their analysis, starting with the effect of throttle input to assess different levels of Accelerator Pedal Pressing (APP) on both vehicle velocity and battery SOC. Following this, the effect of coasting is explored, where the movement of a vehicle without active acceleration or braking is analysed, particularly comparing systems with and without RBS. Next, the effect of braking is evaluated by observing how different levels of BPP influence vehicle deceleration and SOC recovery. Lastly, an analysis of different braking profiles is conducted to investigate how various braking patterns affect energy harvesting and passenger comfort, highlighting the role of braking strategies in maximising RBS efficiency.

3.1 Effect of Throttle Input

Figure 16 presents the open-loop response of the developed mathematical model over 100 seconds. In Figure 16(a), three throttle input scenarios are simulated by varying the APP to 30%, 60%, and 100%. The corresponding velocity responses are shown in Figure 16(b). At 100% AP depression, the maximum velocity reached 13.7 m/s (49.3 km/h), while at 60% depression, the velocity stabilised at 10.5 m/s (37.8 km/h), and at 30%, the velocity was 7.2 m/s (25.9 km/h). The comparison of steady-state values confirms the nonlinear nature of the model, as the velocity increase is not proportional to the percentage of throttle input. This suggests that factors such as aerodynamic drag and drivetrain inefficiencies play a role in limiting the velocity gains at higher throttle inputs. Figure 16(c) presents the SOC over time, starting with an initial SOC of 95%. The SOC decreases linearly but at varying rates depending on the throttle input. For a 30% throttle press, the SOC drops by 0.32% after 100 seconds, for a 60% press, the SOC decreases by 0.63%, and at full throttle (100%), the SOC declines by 1.16%. These findings are consistent with expectations, as increasing throttle input causes the motor to demand more current, thereby accelerating the depletion of battery charge. This occurs because higher throttle inputs signal the controller to increase motor torque, which requires greater electrical power. Since power is the product of current and voltage, and the voltage is constant in most EV battery systems, the system responds by drawing more current. This increased current accelerates the discharge of the battery, leading to a more rapid decline in the SOC.

The results highlight the trade-off between velocity and energy consumption in EVs, where higher speeds result in a more rapid depletion of the battery. The nonlinear velocity response is particularly important for future controller design, as it suggests that linear control strategies may not be effective in maximising performance and energy efficiency simultaneously. The approximately linear decrease in SOC across varying throttle levels emphasises the critical role of throttle management in prolonging battery life. This has direct implications for EV design and energy planning, particularly in sizing the battery pack. If the battery capacity is not carefully matched to expected throttle usage patterns and driving conditions, the vehicle may fail to meet its intended mileage range. For instance, even a modest increase in average throttle input can disproportionately reduce usable driving range. Therefore, selecting an appropriate battery capacity should consider not only peak performance demands but also typical usage profiles and braking recovery potential to achieve a balanced energy strategy. In addition, EV design should incorporate adaptive throttle pedal adjustment mechanisms that limit unnecessary or excessive throttle input, helping to moderate energy consumption and preserve battery health over time. To better illustrate the relationship between throttle input, velocity, and SOC depletion, Table 4 below summarizes the key findings.

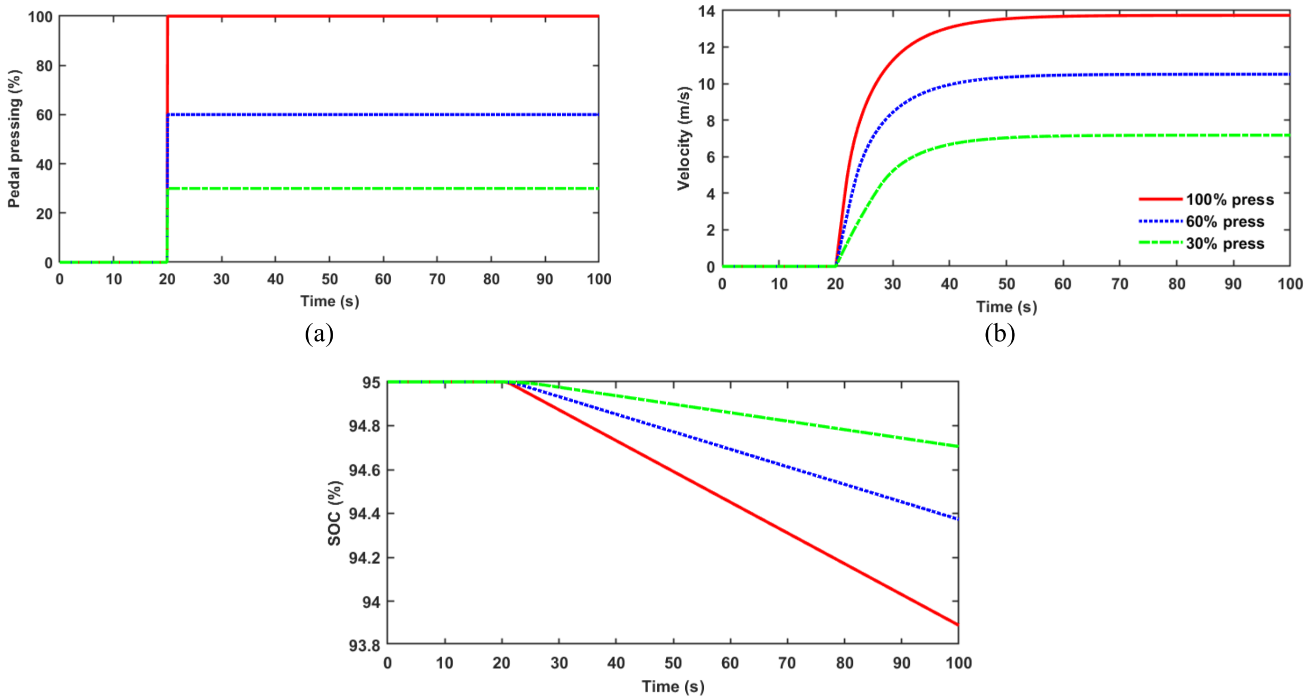

(a) (b) (c)

Figure 16. Effect of (a) throttle pressing percentage (30%, 60%, 100%) over time; (b) vehicle velocity, and (c) battery SOC

Table 4. Summary of findings for effect of throttle input

Throttle Input (%)	Velocity (m/s)	Velocity (km/h)	SOC Depletion (%)
30	7.2	25.9	0.32
60	10.5	37.8	0.63
100	13.7	49.3	1.16

3.2 Effect of Coasting

As discussed before, coasting refers to the condition where a vehicle maintains its speed after the AP is released without applying the BP. In this simulation, the go-kart entered coasting mode after 50 seconds of travel from 100% APP. Two scenarios were analysed: one with a Regenerative Braking System (RBS) and one without it, as illustrated in Figure 17(a). Figure 17(b) shows that the go-kart without RBS experiences a gradual decline in velocity, coming to a complete stop after 35 seconds. In contrast, the go-kart equipped with RBS decelerates more rapidly due to motor braking, stopping after just 20 seconds. This rapid deceleration is caused by the resistance effect from the motor's magnetic induction, which generates electricity during AP release.

Additionally, as shown in Figure 17(c), the battery's SOC for the go-kart with RBS shows a brief increase for approximately 10 seconds immediately after the AP is released. This increase in SOC, although small (0.05%), is a clear indication of energy recovery during the coasting phase. Over time, such incremental improvements in SOC contribute to extending the battery's overall charge duration, effectively enhancing the vehicle's range. Even though the RBS contribution to SOC may seem minor, its cumulative impact on energy conservation may be significant, as RBS improves energy efficiency by harnessing otherwise wasted kinetic energy during coasting.

The go-kart with RBS not only stops faster due to motor braking but also benefits from the small increase in SOC, which contributes to the vehicle's overall energy efficiency and range over time [39]. The observed SOC gain during coasting is explained through the underlying mechanism of regenerative braking, converting kinetic energy into electrical energy stored in the battery. This phenomenon corroborates previous research in [40]–[42], highlighting regenerative braking as crucial for range extension in EVs. These results highlight the advantages of RBS in enhancing energy usage during coasting. From a practical perspective, the implementation of RBS also helps reduce friction brake pad wear, thereby extending the brake pad replacement interval. However, it is worth noting that RBS can alter the natural coasting sensation experienced by drivers familiar with conventional internal combustion engine (ICE) vehicles. In ICE vehicles, coasting typically results in a more gliding sensation due to minimal resistance, whereas RBS introduces noticeable deceleration during coasting, giving a feeling closer to light braking. This change in coasting behaviour may affect driver comfort and expectations, particularly in transitioning from ICE to EV platforms [43]. To summarize the result, Table 5 demonstrates the differences in performance between the two scenarios.

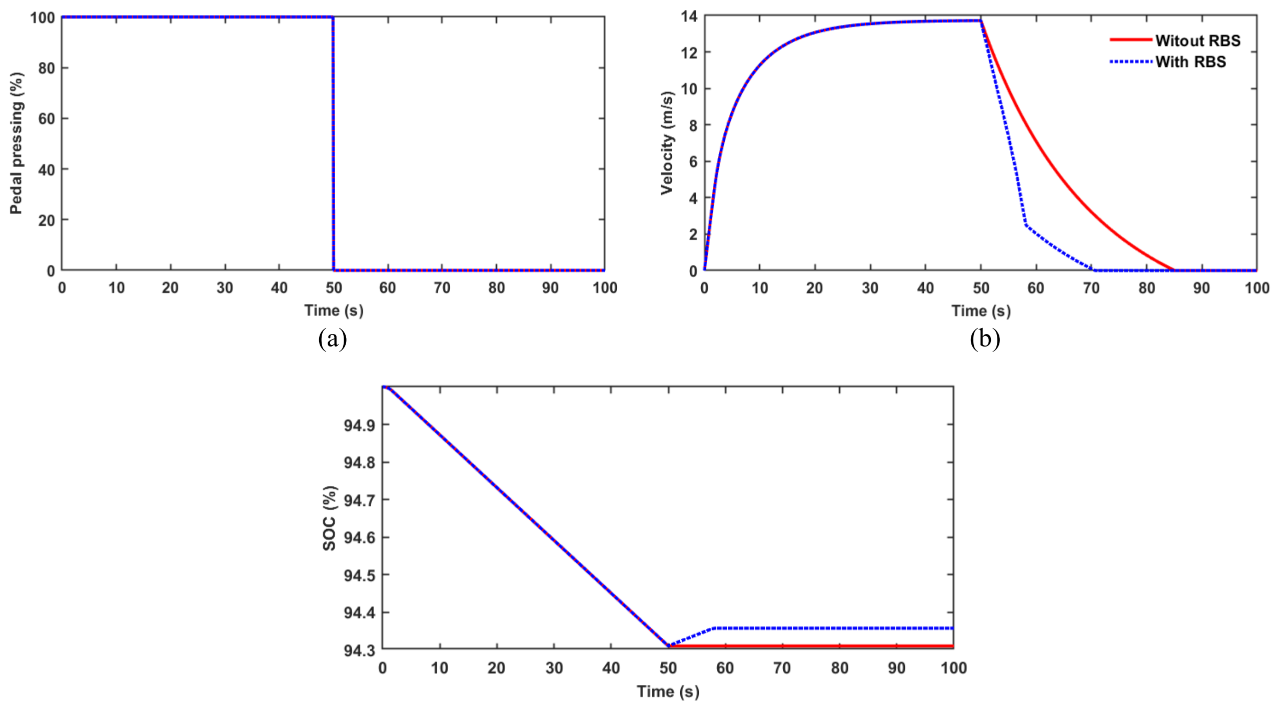

(c)

Figure 17. Effect of (a) coasting mode starts at 50 seconds time on (b) vehicle velocity, and (c) battery SOC

Table 5. Summary of findings for effect of coasting

Condition	Time to stop (s)	SOC change (%)	Velocity decay profile	Energy recovery contribution
Without RBS	35	0	Gradual	None
With RBS	20	+0.05	Rapid (due to motor braking)	Yes (small, but cumulative)

3.3 Effect of Braking

While coasting naturally reduces vehicle speed, friction braking is still required for quicker deceleration. In the EV market, some vehicles integrate RBS within their braking system by distributing braking force between the friction brake and regenerative braking, optimizing both deceleration and energy recovery. However, in the case of this go-kart model, the SRBS system relies entirely on the friction brake for abrupt stopping. Figure 18(a) presents the effects of different BPP on velocity and SOC. In the first graph, positive values indicate APP, while negative values represent BPP. Initially, the AP is fully pressed for the first 50 seconds, followed by varying brake applications. The red line represents coasting without a brake, the blue line shows a 10% BPP, and the green line represents a 50% BPP. As shown in Figure 18(b), coasting takes approximately 20 seconds to bring the vehicle to a complete stop, whereas 10% and 50% BPP result in much faster deceleration, approximately around 2 seconds and 0.5 seconds, respectively.

However, as illustrated in Figure 18(c), rapid braking substantially reduces the energy recovery potential of the RBS, as indicated by a lower increase in SOC compared to the coasting scenario. When the brake is pressed at 50%, the SOC shows minimal increase, reflecting limited energy harvesting. Similarly, with a 10% brake application, there is some improvement in SOC, but it is still not comparable to the 0.05% SOC increase observed during coasting. These results clearly demonstrate how different levels of brake application impact both velocity and battery SOC in an electric vehicle. The data suggests that higher brake application leads to faster deceleration but results in lower SOC gains. Conversely, during coasting, kinetic energy from the wheels is efficiently converted to electrical energy, increasing the SOC, as no energy is dissipated through friction. This behavior highlights a critical trade-off in energy recovery: friction braking reduces the available kinetic energy that could otherwise be converted into electricity via RBS. Once the friction brake is applied, the kinetic energy is rapidly diminished, leading to reduced electricity generation. Importantly, these results reinforce that regenerative braking effectiveness is highly sensitive to braking intensity. In the absence of blended control, a Combined Serial RBS strategy as used in this study limits energy recovery when friction braking dominates [20]. Thus, from a design and control perspective, optimising braking profiles to favor coasting or low-level regenerative braking before friction braking engages can significantly enhance energy efficiency.

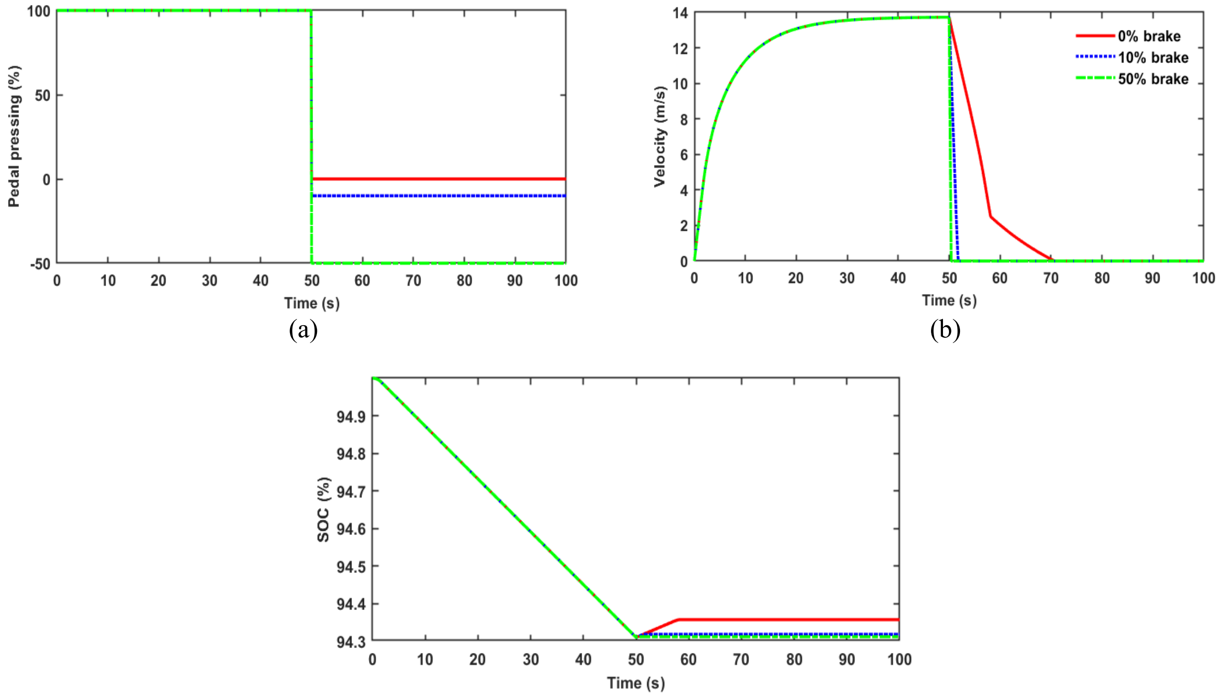

Figure 18. Effect of (a) brake pressing percentage (0%, 10%, 50%) over time on (b) vehicle velocity, and (c) battery SOC

Moreover, in real-world driving, this suggests that an intelligent braking controller should dynamically manage the transition between regenerative and friction braking. Such a system could preserve user comfort while maximising energy recovery, especially in urban stop-and-go conditions where deceleration events are frequent. Table 6 summarizes the braking analysis for this section. From the findings, it is noted that to maximise the RBS efficiency, modulation between coasting, regenerative braking, and friction braking is needed.

Table 6. Summary of findings for effect of braking

Braking condition	Time to stop (s)	SOC change (%)
Coasting	20	+0.05
10% brake	2	+0.009
50% brake	0.5	Minimal

3.4 Analysis of Different Braking Profiles

This section examines the effects of different braking profiles, where the proportion of coasting and friction braking varies. Figure 19 (a) illustrates the response for four distinct brake profiles. Each profile begins with a full AP application until (t = 50 s), followed by different braking patterns designed to manually bring the go-kart to a complete stop by (t = 55 s). The green line represents brake profile 1, in which the BP is pressed continuously at 2.5% after the AP is released. The red line represents brake profile 2, where the go-kart coasts for the first 3 s after throttle release, followed by stronger braking (-5.8% pedal pressing). The blue line represents brake profile 3, which also involves a 3 s coasting period but with a slightly stronger braking force (-7.5% pedal pressing). Finally, the black line represents brake profile 4, where the go-kart coasts for approximately 4 s before applying the strongest braking force (-20% pedal pressing). The resulting velocity responses are shown in Figure 19 (b). All profiles succeed in stopping the vehicle by t = 55 s, but the deceleration patterns differ. Profile 1 shows a smooth and nearly linear velocity decrease due to the absence of coasting. In contrast, Profile 4 features a more gradual decline initially, followed by a sharp drop near t = 54.5 s due to the late application of high brake force. Profiles 2 and 3 produce intermediate deceleration behaviors, with slight differences in intensity and timing that lead to minor variations in the velocity curves.

To assess passenger comfort, Figure 19 (c) plots the acceleration over time. Initially, there is positive acceleration or steady speed (from t=0 to t=50 s), followed by a sharp drop into negative values during braking (from t=50 to t=55 s). The curves reveal peak deceleration before settling as the go-kart stops between (t = 55 s and 100 s). The black line (profile 4) shows the highest deceleration rate of -11.7 m/s², despite having only mild deceleration (-1.3 m/s²) during the cruising phase. The green line (profile 1) displays the lowest deceleration due to light braking, although without coasting. The red and blue lines (profiles 2 and 3) exhibit moderate maximum decelerations of -5.6 m/s² and -6.4 m/s², respectively, with the blue line providing a smoother and more comfortable deceleration experience. Figure 19 (d) displays the SOC evolution for all brake profiles. Following full-throttle operation, all profiles show a slight SOC increase after t = 50 s, reflecting limited energy recovery during the braking phase. The black line (profile 4), which involves the longest coasting period, yields the highest SOC gain, albeit at the cost of a less comfortable ride. In contrast, the green line (profile 1) shows the lowest SOC gain, with a negligible difference of 0.02%. The blue and red profiles (2 and 3) display modest SOC increases, though they are less efficient than the black line in terms of energy recovery.

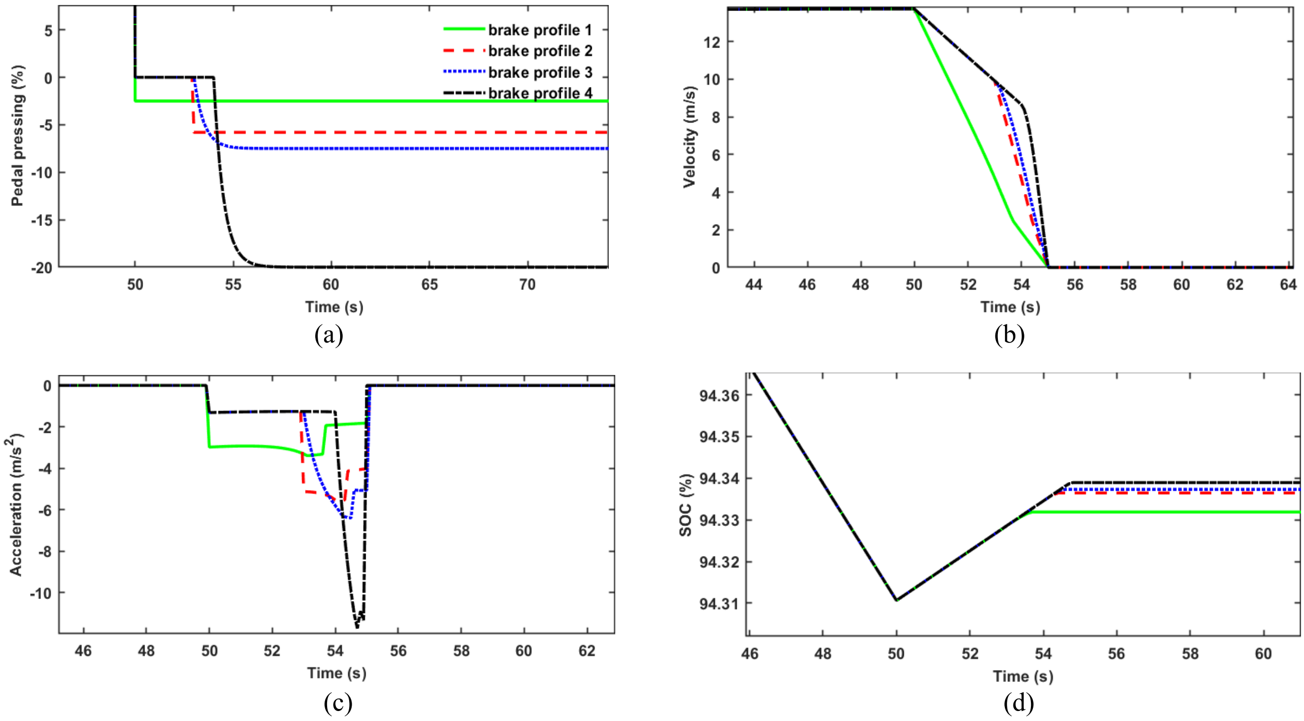

Figure 19. Effect of different brake profiles on (b) velocity, (c) acceleration, and (d) SOC

The results indicate that optimal energy harvesting through the magnetic induction of the traction motor is achieved when the go-kart coasts before braking is applied [39]. To further interpret the practical implications of the SOC results, consider the maximum SOC gain of approximately 0.03% observed in the most aggressive regenerative braking scenario (Profile 4). To put this into perspective, recall the open-loop throttle test results from Section 3.1, where a moderate throttle input of 30% led to an SOC depletion of about 0.32% over 80 seconds. By establishing this baseline, a 0.03% SOC recovery from a single braking event translates roughly into an additional 7.5 seconds of driving time under similar moderate throttle conditions. Although this individual recovery may appear minimal, it is important to highlight that regenerative braking occurs frequently during typical driving conditions, particularly in urban or stop-and-go scenarios. Consequently, the cumulative effect of multiple regenerative braking events can significantly contribute to the overall extension of driving range and improved energy efficiency. Thus, while each single braking event yields a small SOC improvement, the aggregate effect throughout an entire driving cycle underscores the substantial potential benefits of optimising regenerative braking strategies. Future research should focus on developing intelligent braking controllers capable of maximizing these incremental energy gains without compromising passenger comfort.

However, the rate of BPP after coasting is crucial for maximising energy recovery while preserving passenger comfort. Achieving this balance is highly challenging, requiring considerable driver skill and experience [43]. Consequently, developing an intelligent controller that can execute the optimal braking profile by balancing the braking smoothness, energy recovery, and passenger comfort is desirable [44], [45]. The strength of this study lies in its use of a simplified yet representative electric go-kart platform, which enables high-resolution simulation of energy dynamics without the complexity of a full-scale vehicle. Moreover, the control-oriented, first-principles modelling approach bridges theoretical rigour with practical controller implementation, making it well-suited for future development of predictive braking algorithms and onboard energy management systems. For clarity of presentation, Table 7 highlights the main findings from this simulation.

Table 7. Summary of findings for effect of braking profiles

Braking profile	Coasting duration (s)	Brake force (%)	Time to stop (s)	Max. deceleration (m/s^2)	SOC change (%)
Profile 1	0	2.5	5	-3.4	+0.023
Profile 2	3	5.8	5	-5.6	+0.027
Profile 3	3	7.5	5	-6.4	+0.028
Profile 4	4	20.0	5	-11.7	+0.030

3.5 Limitations of the Study

While the developed model offers a control-oriented and practical framework for simulating electric go-kart dynamics and regenerative braking behaviour, several limitations must be acknowledged. First, the model has not been validated with real-world data. As this study focuses on the conceptual analysis of braking strategies, a theoretical approach was adopted. Future work will include experimental validation once the go-kart prototype is fully instrumented with sensors and actuators, enabling accurate model tuning and verification against physical performance data. Despite its theoretical nature, the model provides valuable insight into braking profile patterns that can inform controller design and energy recovery strategies. Second, the simulation uses step inputs for throttle and braking rather than a representative driving cycle. This limits the ability to observe cumulative SOC recovery under real-world conditions. Currently, no standardised go-kart drive cycle is available in MATLAB Simulink, which presents a constraint for realistic scenario testing. Third, parameters such as torque damping coefficients, aerodynamic drag, brake gain and rolling resistance were partially estimated using standard references when direct measurement was impractical. While sufficient for capturing dominant dynamics, this approach may overlook second-order effects. These limitations represent necessary trade-offs to ensure a manageable and interpretable model suitable for early-stage strategy development. Future work will address these issues by integrating experimental validation and implementing a realistic drive cycle. Finally, it is important to emphasise that the focus of this research is to justify the importance of braking profile selection on regenerative braking performance. Therefore, the model assumes fixed vehicle and environmental parameters to isolate the effects of braking strategies. Parameter variations such as changes in mass or drag coefficient were intentionally excluded and are expected to be managed in future work through the application of closed-loop control systems capable of real-time adaptation.

4. CONCLUSION

This study developed a control-oriented, first-principles model of an electric go-kart in MATLAB Simulink to assess the effects of throttle input, coasting, braking intensity, and braking profiles on vehicle dynamics and regenerative braking performance. The model incorporated real-prototype parameters and included subsystems for motor behaviour, vehicle longitudinal dynamics, drivetrain, braking, and battery SOC estimation. It effectively captured the nonlinear relationship between throttle input and velocity, as well as the associated impacts on battery SOC. This model provides a valuable tool for simulating and optimising the dynamics of small-scale electric vehicles, like go-karts, making it applicable for future studies in control development and energy management strategies. Simulation results revealed that increasing throttle input from 30% to 100% raised velocity from 7.2 m/s to 13.7 m/s, with corresponding SOC depletion rising from 0.32% to 1.16%. Energy recovery through regenerative braking is maximised when coasting is emphasised before friction braking is applied, where the system recovered up to 0.05% SOC but with the highest deceleration of -11.7 m/s^2. SOC recovery is sensitive to braking intensity, and excessive reliance on friction brakes diminishes energy harvesting potential. Moderate braking profiles combining coasting and stronger braking achieved up to 0.028% SOC recovery, though with lower peak deceleration values (up to -5.6 m/s^2). These findings highlight trade-offs between energy recovery and ride comfort, and the importance of braking strategy in maximising RBS efficiency. Thus, this study has highlighted the necessity for intelligent braking controllers, which could dynamically adjust the braking force to enhance energy efficiency without compromising the ride experience. From a user experience perspective, regenerative braking modifies the coasting feel, requiring adaptation for drivers accustomed to the gliding behaviour of conventional ICE vehicles. Improvements implemented in this study include the integration of a complete system-level model with regenerative braking logic, conditional friction braking behaviour, and SOC estimation based on motor power characteristics. These enhancements enabled a more realistic analysis of energy flow and dynamic response under varying control inputs. Future work should focus on developing such intelligent controllers capable of adapting brake intensity based on driving conditions to ensure maximum energy recovery and a smooth, comfortable ride.

ACKNOWLEDGEMENTS

The first author gratefully acknowledges the financial support provided by the Ministry of Higher Education Malaysia and Universiti Teknikal Malaysia Melaka (UTeM) for enabling the pursuit of further studies. The authors thank the Ministry of Higher Education Malaysia for the research grant FRGS/1/2019/TK07/UIAM/03/1. This support has been instrumental in the successful completion of this research.

CONFLICT OF INTEREST

The authors declare no conflicts of interest.

AUTHORS CONTRIBUTION

K. A. Tofrowaih (Methodology, Investigation; Data analysis, Writing - original draft, Resources)

M. Abdullah (Conceptualization, Formal analysis; Writing - review & editing, Visualisation; Supervision)

S. F. Toha (Supervision, Project administration, Funding acquisition, Resources, Writing - review & editing)

A. Rahman (Supervision, Consultation on the Concept, Writing - review & editing)

REFERENCES

[1] R. P. Tapaskar, P. P. Revankar, and S. V. Ganachari, "Advancements in battery management systems for electric vehicles: A MATLAB-based simulation of 4S3P lithium-ion battery packs," *World Electric Vehicle Journal*, vol. 15, no. 6, pp. 222–248, 2024.

[2] A. F. Challoob, N. A. Bin Rahmat, V. K. A/L Ramachandaramurthy, and A. J. Humaidi, "Energy and battery management systems for electrical vehicles: A comprehensive review & recommendations," *Energy Exploration & Exploitation*, vol. 42, no. 1, pp. 341–372, 2024.

[3] Y. Ortiz, P. Arévalo, D. Peña, and F. Jurado, "Recent advances in thermal management strategies for lithium-ion batteries: A comprehensive review," *Batteries*, vol. 10, no. 3, pp. 83–103, 2024.

[4] A. Rahmani, M. Dibaj, and M. Akrami, "Recent advancements in battery thermal management systems for enhanced performance of li-ion batteries: A comprehensive review," *Batteries*, vol. 10, no. 8, pp. 265–293, 2024.

[5] A. Afzal, R. K. Abdul Razak, A. D. Mohammed Samee, R. Kumar, Ü. Ağbulut, and S. G. Park, "A critical review on renewable battery thermal management system using heat pipes," *Journal of Thermal Analysis and Calorimetry*, vol. 148, pp. 8403–8442, 2023.

[6] A. Elgammal, "Energy optimization in EV battery thermal management using model predictive control," *International Journal of Scientific Modern Research and Technology*, vol. 4, no. 5, pp. 30–37, 2025.

[7] J. D. O. Velasquez, J. A. G. Moreno, and N. L. D. Aldana, "Experimental platform for studying energy regeneration in electric vehicle powertrains," *Journal of Power Electronics*, vol. 24, pp. 1751–1765, 2024.

[8] R. Islam, S. M. S. H. Rafin, and O. A. Mohammed, "Comprehensive review of power electronic converters in electric vehicle applications," *Forecasting*, vol. 5, pp. 22–80, 2023.

[9] X. Zhai, H. Liu, W. Sun, and Z. Su, "Research on intelligent energy management strategies for connected range-extended electric vehicles based on multi-source information," *Scientific Reports*, vol. 15, no. 1, pp. 12758–12774, 2025.

[10] F. Ji, Y. Pan, Y. Zhou, F. Du, Q. Zhang, and G. Li, "Energy recovery based on pedal situation for regenerative braking system of electric vehicle," *Vehicle System Dynamics*, vol. 58, no. 1, pp. 144–173, 2020.

[11] P. Bathala, B. S. Srivasthav, Y. Sai Srinivas Reddy, and K. Deepa, "Estimation of regenerative braking force in electric vehicles for maximum energy recovery," *2020 IEEE 17th India Council International Conference (INDICON)*, pp. 1–7, 2020.

[12] S. Heydari, "Maximizing Energy Harvesting in Electric Vehicles through Optimal Regenerative Braking Utilization," (Doctoral dissertation, University of Nevada, Reno).

[13] M. J. Yang, H. L. Jhou, B. Y. Ma, and K. Ka. Shyu, "A cost-effective method of electric brake with energy regeneration for electric vehicles," *IEEE Transactions on Industrial Electronics*, vol. 56, no. 6, pp. 2203–2212, 2009.

[14] J. Valladolid, M. Calle, and A. Guiracocha, "Analysis of Regenerative Braking Efficiency in an Electric Vehicle Through Experimental Tests," *Ingenius*, no. 29, pp. 24–31, 2023.

[15] G. A. Chandak and A. A. Bhole, "A review on regenerative braking methodology in electric vehicle," *International Conference Innovations Power Advanced Computing Technologist [i-PACT2017]*, pp. 1265–1269, 2017.

[16] T. Yabe, K. Akatsu, N. Okui, T. Niikuni, and T. Kawai, "Efficiency improvement of regenerative energy for an EV," *26th International Electric Vehicle Symposium (EVS26)*, vol. 1, pp. 634–640, 2012.

[17] H. Faghihian and A. Sargolzaei, "A novel energy-efficient automated regenerative braking system," *Applied Energy*, vol. 390, pp. 125746–125760, 2025.

[18] A. K. Ghazali, M. K. Hassan, M. A. M. Radzi, and A. As'arry, "Optimizing Energy Harvesting: A Gain-Scheduled Braking System for Electric Vehicles with Enhanced State of Charge and Efficiency," *Energies*, vol. 16, no. 12, 2023.

[19] A. Mamgai, "Regenerative Braking Systems (RBS)," *International Journal of Applied Science and Technology*, vol. 6, no. 7, pp. 207–210, 2021.

[20] R. Kubaisi, "Adaptive regenerative braking in electric vehicles," Adaptive Regenerative Braking in Electric Vehicles (Doctoral dissertation, Karlsruher Institut für Technologie (KIT), 2018.

[21] C. Wang, X. Zhao, R. Fu, and Z. Li, "Research on the comfort of vehicle passengers considering the vehicle motion state and passenger physiological characteristics: Improving the passenger comfort of autonomous vehicles," *International Journal of Environmental Research and Public Health*, vol. 17, pp. 6821–6840, 2020.

[22] A. K. Ghazali, M. K. Hassan, M. Amran, and M. Radzi, "Optimizing energy harvesting: A gain-scheduled braking," *Energies*, vol. 16, pp. 4561–4580, 2023.

[23] C. C. Chan, A. Bouscayrol, and K. Chen, "Electric, hybrid, and fuel-cell vehicles: Architectures and modeling," *IEEE Transactions on Vehicular Technology*, vol. 59, no. 2, pp. 589–598, 2010.

[24] D. W. Gao, C. Mi, and A. Emadi, "Modeling and simulation of electric and hybrid vehicles," *Proceedings of the IEEE*, vol. 95, no. 4, pp. 729–745, 2007.

[25] F. Zendri, R. Antonello, F. Biral, and H. Fujimoto, "Modeling, identification and validation of an electric vehicle for model-based control design," *International Workshop on Advanced Motion Control*, pp. 118–123, 2010.

[26] M. M. Gulzar, B. Sharif, D. Sibtain, L. Akbar, and A. Akhtar, "Modelling and controller design of automotive cruise control system using hybrid model predictive controller," *15th International Conference on Emerging Technologies*, pp. 329–333, 2019.

[27] A. Agrawal *et al.*, "Mathematical modeling of driving forces of an electric vehicle for sustainable operation," *IEEE Access*, vol. 11, pp. 95278–95294, 2023.

[28] C. F. Kusuma, B. A. Budiman, and I. P. Nurprasetio, "Simulation method for extended-range electric vehicle battery state of charge and energy consumption simulation based on driving cycle," *ICEVT 2019 - 2019 6th International Conference on Electric Vehicular Technology*, pp. 336–344, 2019.

[29] M. R. Wahid, E. Joelianto, and N. A. Azis, "System Identification of Switched Reluctance Motor (SRM) Using Black Box Method for Electric Vehicle Speed Control System," *2019 6th International Conference on Electric Vehicular Technology*, pp. 208–212, 2019.

[30] S. K. Sunori, M. C. Lohani, S. Maurya, M. Manu, S. Arora, A. Mittal, et al., "Model identification of electric vehicle system," *2022 Sixth International Conference on I-SMAC (IoT in Social, Mobile, Analytics and Cloud)(I-SMAC*, pp. 847–851, 2022.

[31] S. Buggaveeti, M. Batra, J. McPhee, and N. Azad, "Longitudinal vehicle dynamics modeling and parameter estimation for plug-in hybrid electric vehicle," *SAE International Journal of Vehicle Dynamics, Stability*, vol. 1, no. 2, pp. 289–297, 2017.

[32] T. A. T. Mohd, M. K. Hassan, and W. M. K. A. Aziz, "Mathematical modeling and simulation of an electric vehicle," *Journal of Mechanical Engineering and Sciences*, vol. 8, pp. 1312–1321, 2015.

[33] "System-Level Battery Electric Vehicle (BEV) Model." https://www.mathworks.com/help/sps/ug/system-level-battery-electric-vehicle-model.html#BEVSystemLevelExample-3

[34] V. Vodovozov, Z. Raud, and E. Petlenkov, "Review on braking energy management in electric vehicles," *Energies*, vol. 14, no. 15, pp. 4477–4503, 2021.

[35] S. Idros, M. Abdullah, S. F. Toha, and M. S. Md Said, "Modelling of vehicle longitudinal dynamics for speed control," *Journal of Advanced Research in Applied Mechanics*, vol. 123, no. 1, pp. 56–74, 2024.

[36] R. Rajamani, *Vehicle Dynamics and Control*, Second Edi. New York: Springer, 2012.

[37] R. N. Jazar, *Vehicle Dynamics: Theory and Application*, Fourth Edi. New York: Springer, 2025.

[38] M. Abdullah, M. A. S. Zainuddin, S. Ahmad, and J. A. Rossiter, "Performance comparison between centralized and hierarchical predictive functional control for adaptive cruise control application," *International Journal of Automotive and Mechanical Engineering*, vol. 20, no. 4, pp. 10808–10820, 2023.

[39] "Proton e.MAS 7: Weekend SPARK Media Drive and Lunar New Year Celebration with 30% Charging Discounts – Proton e.MAS," 2025. https://emas.proton.com/proton-e-mas-7-weekend-spark-media-drive-and-lunar-new-year-celebration-with-30-charging-discounts/ (accessed Mar. 26, 2025).

[40] V. Vodovozov, Z. Raud, and E. Petlenkov, "Comparative analysis of intelligent braking controllers for electric vehicles," *Renewable Energy and Power Quality Journal*, vol. 20, pp. 55-60, 2022.

[41] S. S. Bhurse and A. A. Bhole, "A review of regenerative braking in electric vehicles," *7th IEEE Sponsored International Conference on Computation of Power, Energy, Information and Communication*, pp. 363–367, 2018.

[42] T. Patil, R. Yadav, A. Mandhare, M. Saggam, and A. Pratap Singh, "Performance improvement of regenerative braking system," *International Journal of Scientific and Engineering Research*, vol. 9, no. 5, pp. 161–165, 2018.

[43] P. Cocron, F. Bühler, T. Franke, I. Neumann, B. Dielmann, and J. F. Krems, "Energy recapture through deceleration - regenerative braking in electric vehicles from a user perspective," *Ergonomics*, vol. 56, no. 8, pp. 1203–1215, 2013.

[44] J. Biao, Z. Xiangwen, W. Yangxiong, and H. Wenchao, "Regenerative braking control strategy of electric vehicles based on braking stability requirements," *International Journal of Automotive Technology*, vol. 22, no. 2, pp. 465 – 473, 2021.

[45] S. Heydari, P. Fajri, M. Rasheduzzaman, and R. Sabzehgar, "Maximizing regenerative braking energy recovery of electric vehicles through dynamic low-speed cutoff point detection," *IEEE Transactions on Transportation Electrification*, vol. 5, no. 1, pp. 262 – 270, 2019.